Study on the Seismic Behavior of the Pile Foundations Supporting a Plate-shaped Building on Clayey Ground

Takehiro Okumura*1 Junji Hamada*2 Tsuyoshi Honda*2

Summary

The seismic behavior of the plate-shaped building supported by pile foundation in soft ground is not clear since the soil non-linearity is significantly complicated and large overturing moment is caused during a large earthquake. This study confirmed that the soft clayey ground can be easily made in a short time in a centrifugal model test by using Kanto Loam as a ground material, and it was confirmed that the clayey ground has a low range of shear wave velocity from 100 m/s to 200 m/s in centrifugal 50g field. Also, the response of plate-shaped building and the stress of pile foundation in clayey ground were observed.

Keywords: pile foundation, clayey ground, centrifugal model test, plate-shaped building

1 Introduction

Since most of the urban areas of Japan have been developed in alluvial plains, buildings are often constructed on soft ground in the bay area, and pile foundations are often used as foundations. However, their behavior during a large earthquake is difficult to predict due to the strong non-linearity of the ground, significant ground deformation, and many other aspects of uncertainty. Furthermore, it is assumed that a plate-shaped building generates a large incremental axial force due to its aspect ratio (height/length in the short-side direction)—the building response changes in a complex manner when the pulling force consistently exceeds the axial force. Dynamic analysis, vibration experiments, and seismic observations have been conducted to date regarding the behavior of pile foundation buildings located on soft ground during earthquakes; as a result, it has been found that dynamic interaction occurs between the building, foundation, and ground[1), 2)]. However, the non-linearity of the ground during a large earthquake has not been thoroughly researched[3)]. Meanwhile, the centrifugal model test is an effective method in vibration experiments that can reproduce the ground behavior during an earthquake. Many experiments have been conducted on pile foundations, including liquefied ground. Previous research with the centrifugal model focused mainly on the sandy ground using silica sand to facilitate the experiments. However, Kishida et al.[4)] measured the shear wave velocity of Toyoura sand in the centrifugal field using a tank with a depth of 250 mm and a bender element. They demonstrated that the average shear wave velocity was higher than 210 m/s at an average normal stress of approximately 98 kPa in a 50 g centrifugal field. In this way, increased centrifugal acceleration increases the confining pressure, making it challenging to reproduce soft ground conditions with a shear wave velocity of less than 200 m/s on dry sandy ground. Since liquefaction occurs when the sand ground is saturated, and the confining pressure is lowered, many soft ground experiments involve the sandy ground's liquefaction. Although pile foundations are often constructed on the soft clayey ground, few experiments have been performed due to the high degree of difficulty in conducting them[5), 6), 7)].

Therefore, we have used Kanto Loam as a cohesive soil material in this study and controlled the maximum dry density and optimal water content ratio. The model ground was manufactured to try a method of producing a soft clayey ground that stabilizes in a short period in a centrifugal field. Furthermore, we have conducted vibration experiments using a ground-only test specimen not containing structures. Additionally, we have identified the ground rigidity and damping from the obtained acceleration. We have confirmed that the centrifugal field's ground rigidity and non-linear characteristics were almost identical to the laboratory test results. Furthermore, we used a plate-shaped building and model that imitated a pile foundation and conducted six cases of dynamic interaction experiments of the building-pile-ground system to investigate the effects of ground conditions and the structure's shape on the pile stress.

*1 Senior Researcher, Research & Development Institute.
*2 Chief Researcher, Research & Development Institute. Dr. Eng.

2 Overall outline of the Experimental method

Fig. 1 shows the schematic diagram of the plate-shaped building's prototype used to plan the centrifugal model experiment. The prototype building was a plate-shaped apartment building (medium/high-rise) with 13 floors above the ground and without basement. The surface ground was a soft and clayey ground with a target shear wave velocity of 100 - 200 m/s. The pile foundation was a cast-in-place concrete pile with a shaft diameter of 1.5 m, an expanded bottom diameter of 2.2 m, and a pile length of 19 m. Table 1 shows a list of the implemented experimental cases. Cases 1-0 to 1-2 were conducted to confirm the validity of the experimental methods, such as making the clayey ground and dynamic behavior. Cases 2-0 to 2-2 involved investigating cases involving liquefied sand layer on the surface, assuming severe conditions due to the building and pile foundation. Case 3-1 involved using a tall model closer to the actual structure to investigate the effect of the moment of inertia of the building on the pile foundations. Case 3-2 involved investigating the influence of the soft clay ground under the thin load-bearing layer.

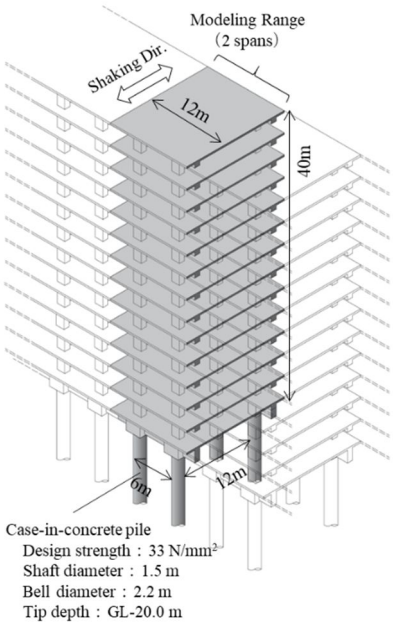

Fig. 1 Schematic diagram of a plate-shaped building's prototype

3 Experiment for performance confirmation of a soft clayey ground

Table 1 List of centrifugal model test cases

Case	Superstructure (Bottom gap)	Load-bearing layer	Liquefiable layer (Method)
1-0	—	Silica sand	—
1-1	Low (—)	Silica sand	—
1-2	Low (○)	Cement treated silica sand	—
2-0	—	Cement treated silica sand	○ (Air pluviation)
2-1	Low (—)	Cement treated silica sand	○ (Air pluviation)
2-2	Low (—)	Cement treated silica sand	○ (Wet tamping)
3-1	High (○)	Cement treated silica sand	—
3-2	High (○)	Cement treated silica sand (with underlying clay layer)	—

One of the challenges of the experiment using soft clayey soil in the centrifugal field is the length of the test period. The conventional preparation of saturated clayey ground involves (1) pre-consolidation in a 1 g field, (2) installation of model and instrument, (3) pre-consolidation in a centrifugal field, and (4) vibration experiments. This takes approximately 1.5 - 2.0 months per case. Furthermore, when a laminar shear box is used in a dynamic model experiment, installing the model and instrument becomes complicated. Additionally, the model and instrument move due to consolidation settlement during the centrifugal field's pre-consolidation process. Therefore, in this study, we decided to shorten the time by using Kanto Loam, a cohesive volcanic ash soil collected at a construction site in Tokyo, as a reconstruction sample and creating a model ground by wet tamping. Kanto Loam has a very high-water retention ratio. Thus, the range of water content that can be retained is very wide at 20 - 100%, and the porosity ratio of the soil can be controlled by the water content ratio, which enables the efficient creation of soft or hard ground in a short period. To understand the material and dynamic deformation characteristics, various tests were conducted to use Kanto Loam as the ground material for the centrifugal model test. A vibration experiment was conducted in a centrifugal field to verify whether the dynamic deformation characteristics obtained in the laboratory test could be reproduced in the centrifugal field.

3.1 Laboratory soil test

We investigated the specifications (i.e., initial water content ratio, compaction density, etc.) for producing soft and viscous ground with Kanto Loam. We conducted dynamic and static mechanical tests assuming stress states in the centrifugal field. Table 2 shows the physical test results of the collected Kanto Loam, and Fig. 2 shows the particle size distribution curve. This sample was volcanic ash sandy cohesive soil with high sand content; it was NP in the consistency test. Fig. 3 shows the results of the soil compaction test. The optimal water content ratio was 63.1%, and the maximum dry density was 0.943 g/cm^3. Based on

Table 2 Summary of Kanto-loam's physical tests

Soil particle density (g/cm^3)	2.599
Sand fraction (%)	31.0
Silt fraction (%)	43.7
Clay fraction (%)	25.3
D50 (mm)	0.0241

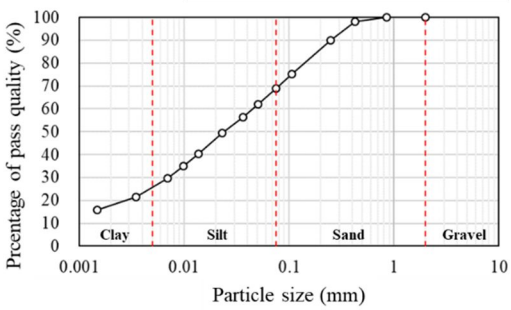

Fig. 2 Grain size distribution curve of Kanto-loam

these results, the test specimens for the centrifugal experiment were prepared with the optimal water content ratio and maximum dry density. The mechanical test was conducted under the confined pressure expected to occur in the centrifugal field of 50 g. In the centrifugal model test, self-consolidation was conducted in a centrifugal field of 50 g after the model ground was prepared. At this time, the sides of the soil tank were under K_0 consolidation conditions constrained by the shear ring. Therefore, a K_0 consolidation test was conducted to determine the earth pressure coefficient under K_0 consolidation conditions. Fig. 4 shows the test results. It was confirmed from the figure that the earth pressure coefficient was approximately 0.3. Since it was expected that the dynamic deformation characteristics of the Kanto Loam ground properties would change depending on the confining pressure of the centrifugal field, a dynamic deformation test was conducted with a triaxial tester under isotropic and anisotropic conditions (K_0 = 0.3) in the normal stress range of 25 - 300 kN/m^2. Table 3 shows the test results. Here, Poisson's ratio ν and dynamic shear rigidity G_d are obtained from the test specimens' measurement results of the P-wave and S-wave velocities. Furthermore, the dynamic shear stiffness G_0 is the isotropic stiffness at the first repeated loading at a strain level of 10^{-3}%. Fig. 5 shows the dynamic deformation characteristics. The normalized shear modulus G/G_0 under our consolidation conditions has the same curve regardless of the confined pressure, except for the result of 25 kN/m^2, which had minor normal stress. It can also be considered that the rate of decrease in rigidity in isotropic and anisotropic states is almost identical. Although there was some variation between the isotropic and anisotropic states, the damping ratio showed nearly the same value up to a strain level of 0.1%. However, the damping ratio tended to increase when the strain level exceeded 0.1% because it approached the fracture state line on the compression side in the anisotropic state.

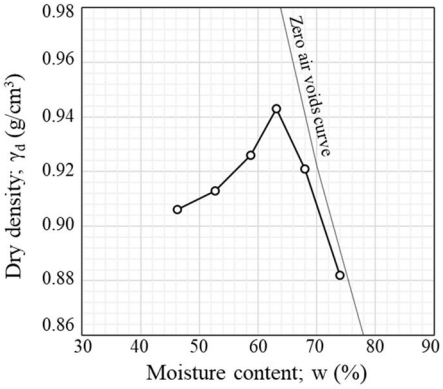

Fig. 3 Moisture-density curve (A-b method)

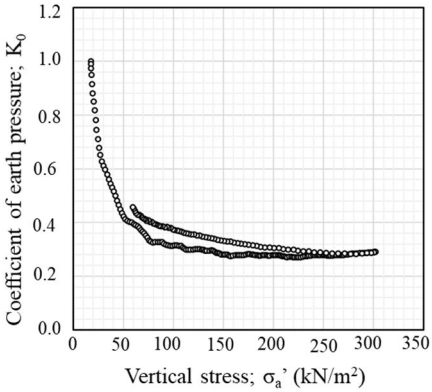

Fig. 4 K_0 consolidation test result

Table 3 Summary of conditions and results of cyclic triaxial test

Consolidation condition	σ'_a kN/m^2	σ'_r kN/m^2	ρ_t g/cm^3	V_p m/s	V_s m/s	ν	σ'_a MN/m^2	σ'_a MN/m^2
Isotropic	25	25	1.577	461	99	0.476	15.5	12.6
	50	50	1.592	474	102	0.476	16.6	16.4
	100	100	1.594	608	152	0.467	36.8	30.7
	200	200	1.593	833	174	0.477	48.2	52.4
Anisotropic	50	21	1.537	700	118	0.485	21.4	16.3
	100	30	1.539	622	166	0.462	42.4	27.1
	200	60	1.550	831	190	0.472	56.0	45.0
	300	90	1.560	984	203	0.478	64.3	60.0

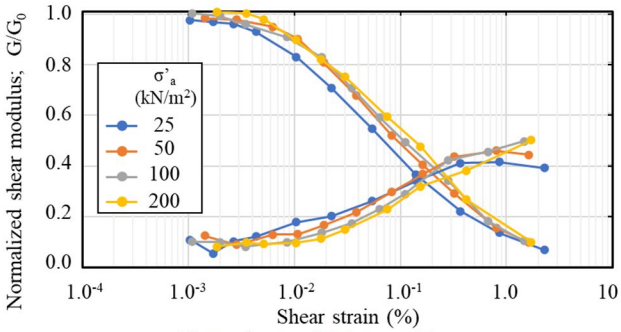

a) Isotropic consolidation condition

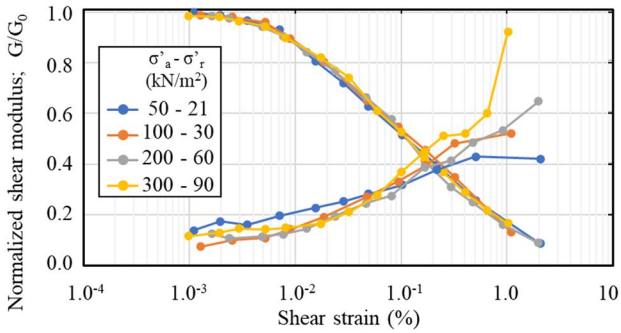

b) Anisotropic consolidation condition

Fig. 5 Dynamic deformation properties by cyclic triaxial test

3.2 Outline of centrifugal model test

Case 1-0, shown in Table 1, was the first experiment to confirm the clayey ground's dynamic deformation characteristics in the centrifugal field. The experimental ground (Case 1-0) shown in Fig. 6 was planned for investigating a field with a centrifugal acceleration of 50 g. The ground was prepared as follows: first, the lower layer was rammed with Iide silica sand No. 4 so that the relative density was 90%, and when this reached a pre-determined height, degassed water was injected from the bottom of the soil tank to saturate it. Water was used for the pore fluid without adjusting the viscosity. This may be due to the low permeability coefficient of Kanto Loam at 9.0 × 10^{-5} cm/s (equivalent to silt) and the slight influence of permeability during vibration. Next, the

upper layer was prepared by ramming Kanto Loam with an adjusted water content ratio (63.1%) every 2 cm to obtain a target density (dry density of 0.943 g/cm^3). Many sensors were placed and measured during the experiments, as shown in Fig. 6, to observe the degree of consolidation progress of the viscous ground and the seismic response. A ceramic filter saturated with 100 cSt silicon oil was used to measure the water pressure in unsaturated soil, particularly for the water pressure gauge. Furthermore, the ground surface was covered with a polyethylene film coated with silicone oil (100 cSt) to prevent the ground from drying out during the experiment.

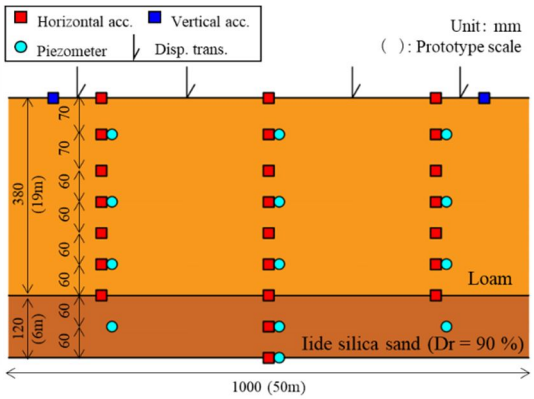

Fig. 6 Schematic diagram of Case 1-0

3.3 Vibration experiment

The vibration experiment was conducted after the clayey ground was consolidated for approximately 6 hours at a centrifugal acceleration field of 50 g. The outcrop base wave (2E wave) that was the basis of the input seismic motion and its acceleration response spectrum was shown in Figs. 7 and 8, respectively. The outcrop motion was a seismic motion that was created using the acceleration response spectrum that was defined as a "sporadic seismic motion" in a notification (Ministry of Construction No. 1461, 2012) for the phase characteristics of the seismic motion (NS component) that was observed at the Kobe Marine Meteorological Observatory at the time of Great Hanshin Earthquake in 1995. The input to the actual shaking table was the within motion (E+F) that was obtained by one-dimensional equivalent linear analysis modeling the model ground, and the acceleration waveform used was that analyzed by standardizing the maximum acceleration of the outcrop base wave to 0.5, 1.5, 2.0, 3.5, 4.5, and 6.0 m/s^2. The analysis does not include the reflected waves due to the structure's vibration, but it was judged that the soil tank was sufficiently large compared to the weight of the structure model used, and its influence could be ignored. Table 4 shows the maximum acceleration of the outcrop base motion and the maximum acceleration of the within base motion in each vibration case.

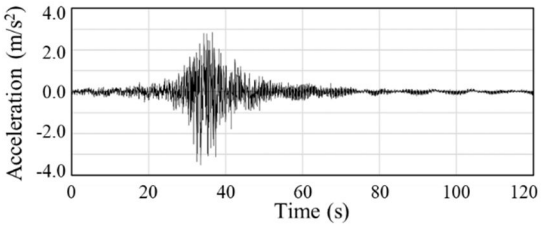

Fig. 7 Time history of input motion (2E)

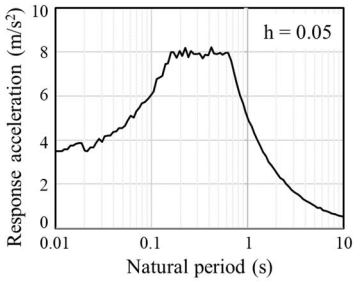

Fig. 8 Response acceleration of input motion (2E)

Table 4 Maximum acceleration of outcrop motion and within motion

Case Index	Max. Acc. (m/s^2)	
	Outcrop (2E)	Within (E+F)
50 Gal	0.50	0.35
150 Gal	1.50	0.89
200 Gal	2.00	1.23
350 Gal	0.50	2.14
450 Gal	0.50	2.96
600 Gal	0.50	3.85

3.4 Identification of ground physical properties based on experimental results

We estimated the clayey ground's shear modulus and damping constant in the centrifugal field by assuming the ground as a one-dimensional multi-mass model and by identifying the shear modulus and damping constant from acceleration records[8]. Fig. 9 shows the amplification characteristics calculated based on the one-dimensional multi-reflection theory from the equivalent shear modulus and damping constant of each layer obtained, ground surface obtained in the vibration experiment, and the acceleration Fourier amplitude spectrum ratio in the shaking table. The ground physical properties identified as shown in Fig. 9 effectively reproduce the primary natural period of the experiment and its amplitude ratio, confirming the validity of this method. Fig. 10 shows the relationship between the equivalent rigidity and strain dependence of the equal

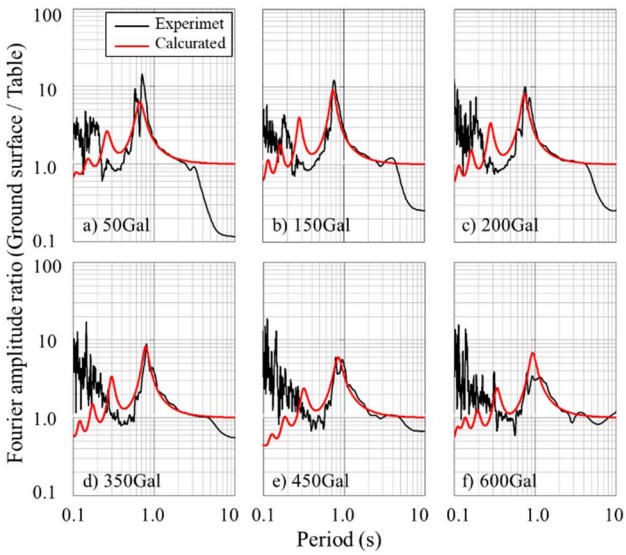

Fig. 9 Fourier amplitude ratio of ground surface against shaking table

damping constant using the maximum shear strain of each layer that was obtained by integrating acceleration records through a 0.5–2.0 Hz bandpass filter, as well as the dynamic deformation test results under isotropic consolidation conditions that are shown in Fig. 5(a) in black dotted lines. In the legend, σ_v' is the effective stress when the groundwater level is GL-11 m from the water pressure record, and σ_c in the figure indicates the confining pressure in the laboratory test. As shown in Fig. 10(a), the strain dependence of the equivalent stiffness tends to be in harmony with the laboratory test results and its confined pressure dependence. Meanwhile, the damping constant is slightly different from the laboratory test results, as shown in Fig. 10(b), but clearly it is almost the same. However, according to this study, the equivalent damping constant also tends to increase from a strain of approximately 0.2%. As seen in the dynamic deformation test results under the anisotropic consolidation condition shown in Fig. 5(b), the material damping tended to increase as the strain increased; hence, it is possible that the material damping was predominant when compared to the dissipation damping. It was confirmed from the above results that a clayey ground with precise specifications could be created relatively quickly in a centrifugal field.

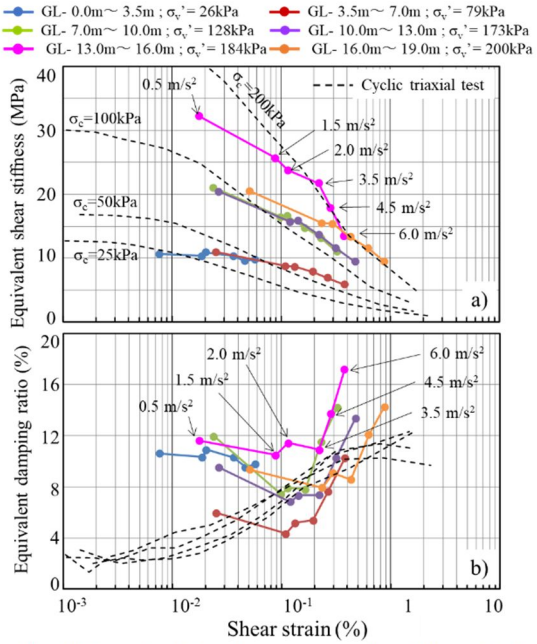

Fig. 10 Dynamic deformation properties of variable confined pressure estimated from the acceleration

4 Vibration experiment of the plate-shaped building–pile–soft ground system

4.1 Outline of the experiment

We confirmed the behavior of the plate-shaped building and pile foundations that support it during an earthquake by conducting an experiment that incorporated a structural model that simulated them. In this study, we have reported the results of Cases 1-2, 2-2, and 3-1 as representative examples of the cases presented in Table 1. Fig. 11 shows the outline of each experiment. In the centrifugal model experiment, vibration was applied in the direction between the beams of the plate-shaped building used as a model, and the two spans (as shown in Fig. 1) in the girder directions were modeled. The modeling of the building for the low-structure model used in Cases 1-2 and 2-2 combined the natural period and constant pile axial force with the prototype using a scaling law of the centrifugal field[9] as a three-layer frame structure from the eigen value analysis at the time of fixing the foundation condition. For the high-structure model used in Case 3-1, the natural period, constant pile axial force, and moment of inertia were combined with the prototype by the scaling law of the centrifugal field as a one-layer truss structure from the eigen value analysis at the time of fixing the foundation condition. The modeling of the pile foundation involved using an aluminum pipe (φ30 mm, t =

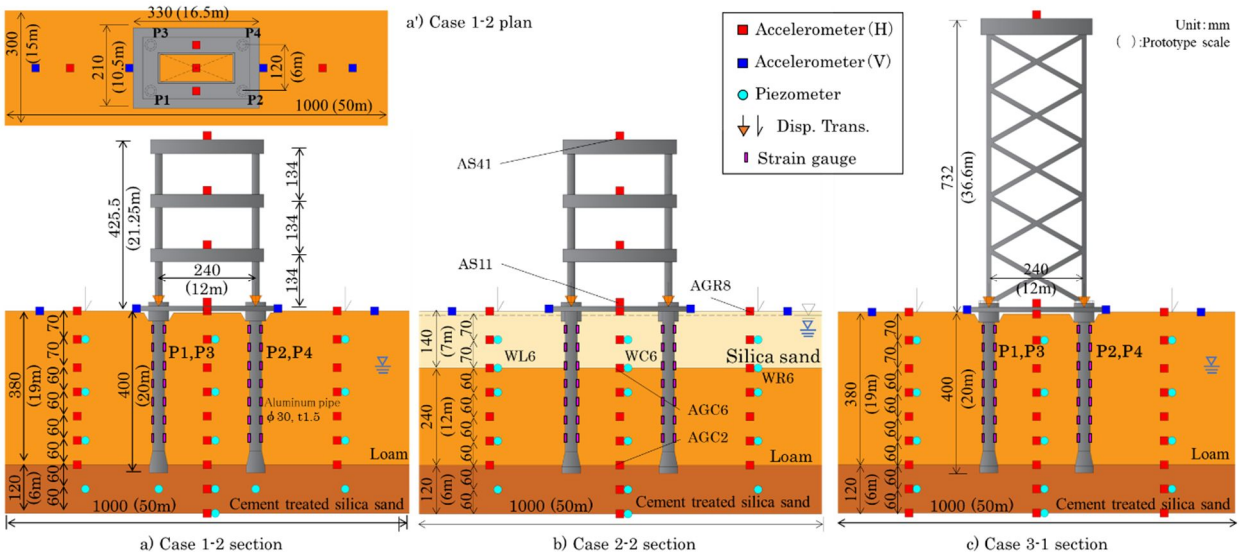

Fig. 11 Schematic diagrams of shaking table tests on superstructure-pile-ground system

1.5 mm) to match the initial rigidity of the shaft against bending to the prototype. Aluminum alloy was used for the expanded bottom part, and the bottom part was connected to the shaft part with an epoxy adhesive. For the model ground, the load-bearing layer used Iide silica sand No. 4 (Dr = 90%) with cement (W/C = 100%) added at 100 kg/m^3 to increase the strength (uniaxial compressive strength; q_u = 1.4 N/mm^2) and rigidity (shear wave velocity; Vs = approx. 550 m/s). The clayey ground was created in the same way as the experiment in the previous section. A notch was provided in the cohesive soil around the pile cap to prevent the lateral force from transmitting from the pile cap to the ground for Cases 1-2 and 3-1. The reason for this is a concern from the analysis of the results of Case 1-1 indicating the flow of a part of the inertial force of the structure from the pile cap and the bottom of the foundation beam to the ground[10]. The liquefied ground provided on the surface layer of Case 2-2 was prepared by wet tamping of the Iide silica sand No. 6 (Dr = 70%). In the wet tamping method, silicone oil was added in advance at an amount that was 5% of the weight of the sand, and after sufficiently stirring it, ramming was conducted. After the ground was prepared by ramming to the ground surface, 50 cSt of degassed silicone oil was infiltrated from the lower end of the liquefaction layer in the air to saturate it. Each test specimen was subjected to centrifugal consolidation for 3–6 h in a centrifugal 50 g field, and vibration experiments were conducted after the ground surface subsidence, and excess pore water pressure became stable. The vibration experiment was performed similarly to Case 1-0, as discussed in section 3.3.

4.2 Building and ground response

Fig. 12 compares the maximum value and input level of each calculated inertial force and the overturning moment from the structure acceleration obtained in the vibration experiment. As shown in the figure, Cases 1-2 and 3-1 had increasing inertial force and overturning moment as the input level increased. Case 2-2 had an increasing inertial force and overturning moment as the input level increased from 50 to 350 Gal input. However, both the inertial force and overturning moment reached a plateau at 600 Gal input, and the values were about the same as at 350 Gal input. The time history of excess pore water pressure observed at the lower end of the liquefaction layer at the input of 200–600 Gal has been represented in Fig. 13 to discuss this result. The black dotted line in the figure shows the total stress at the installation depth of the water pressure gauge, and it is assumed that liquefaction occurred in the part where the excess pore water pressure reached the total stress. It is evident from the figure that the increase in excess pore water pressure in the ground between piles (Fig. 13(b)) was more significant than that in the surrounding ground (Fig. 13(a), (c)). The reason for this may be the transmission of the inertial force of the building to the ground through the piles and an increase in the shear strain of the ground as a result. Additionally, the ground between the piles was liquefied when 350 Gal was input, but there is the possibility that the surrounding ground did not liquefy. Furthermore, the 600 Gal input involved the liquefaction of the surrounding ground. Fig. 14 shows the maximum acceleration distribution when 600 Gal was input. Fig. 15 also shows the maximum value distribution of the displacement obtained by the second-order integration of these acceleration records (Trifunac's method[11]). It was also confirmed that the displacement waveform obtained by this method from the acceleration record measured by the shaking table was almost the same as the displacement waveform that was directly measured by the gap sensor. Cases 1-2 and 3-1 (Fig. 14(a), (c)) had an amplifying tendency from GL-7.0 m to the ground surface. However, Case 2-2 (Fig. 14(b)) had a decreasing trend for the acceleration at a shallower point than at the GL-7.0 m

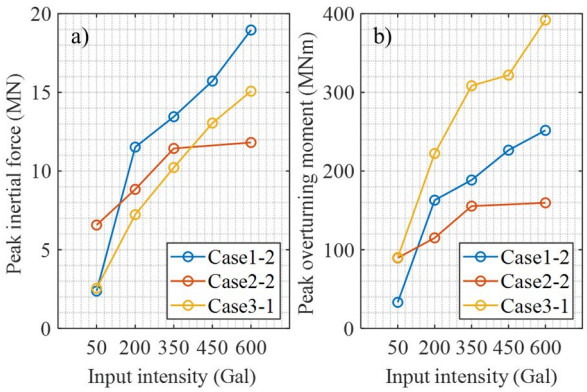

Fig. 12 Peak inertial force and Peak overturning moment of superstructure against input intensity

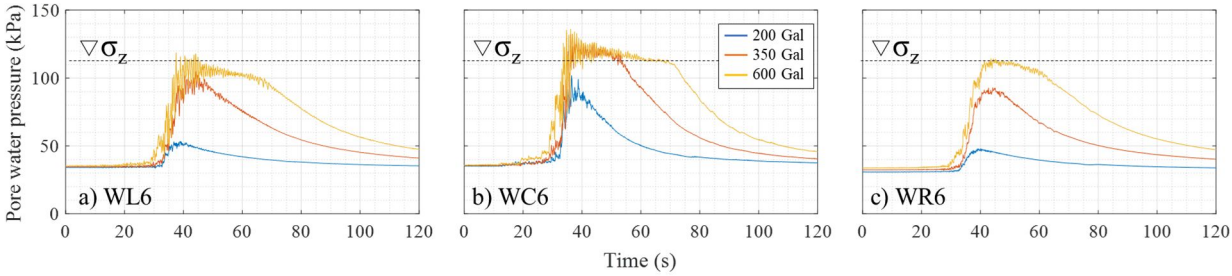

Fig. 13 Time records of pore water pressure observed at the bottom of liquefiable layer

point. It can be observed in Cases 1-2 and 3-1 (Fig. 15(a), (c)) that the maximum displacement gradually decreased from GL-7.0 m toward the ground surface. Meanwhile, clearly in Case 2-2 (Fig. 15(b)), the maximum displacement increased significantly between GL-7.0 m and GL-3.5 m. Subsequently, a comparison between the ground acceleration (ground surface acceleration) and structure acceleration (foundation acceleration) at an altitude of GL+0 m showed that, in Case 1-2 (Fig. 14(a)), despite variable ground surface acceleration depending on the installation position, the ground surface acceleration and foundation acceleration were almost identical in all experiments. From the above results, it is thought that the 600 Gal input in Case 2-2 resulted in a decreased shear rigidity and damping of the short-period component of the acceleration due to the liquefaction of the sandy ground between GL-3.5 and 7.0 m. As a result, the input acceleration was damping the structure, with the inertial force and overturning moment reaching a plateau from 350 to 600 Gal input. Comparing Cases 1-2 and 3-1, the structural inertial force (Fig. 12(a)) was slightly smaller in Case 3-1 than in Case 1-2. As shown in Figs. 14(a) and (c), the foundation acceleration was around 7.0 m/s^2 for both Cases 1-2 and 3-1; the building top acceleration was slightly amplified relative to that of the foundation at around 8.0 m/s^2 for Case 1-2, but this was damped comparable to that of the foundation at around 4.5 m/s^2 for Case 3-1.

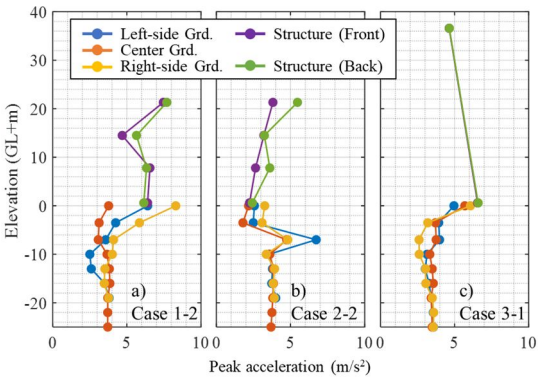

Fig. 14 Peak acceleration distribution observed in shaking table test of 600 Gal

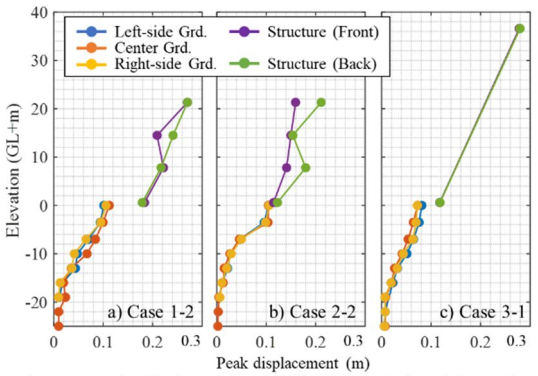

Fig. 15 Peak displacement distribution calculated by 2nd integration of acceleration observed in shaking table test of 600 Gal

Meanwhile, when comparing the maximum displacement, Cases 1-2 and 3-1 had a building top displacement of around 0.3 m. Hence, it was inferred that the building top acceleration in Case 3-1 had a more extended period than that in Case 1-2. The superstructure model used in Cases 1-2 and 3-1 had the same natural period when the foundation was fixed, but the inertial moment doubled from Case 1-2 to Case 3-1. Thus, it is thought that the rocking motion of the superstructure had an extended period. It is believed from the above results that a significant moment of inertia of the superstructure resulted in more extended rocking motion and damping of the top acceleration, reducing the inertial force of the structure. However, it is possible that the overturning moment remained large due to the significant moment of inertia, although the maximum acceleration became small.

4.3 Stress generated in pile foundation

The bending moment-axial force correlation diagram (M-N correlation diagram) at the pile head at 600 Gal input is shown in Fig. 16 to compare the pile stress that was generated in each experiment. The axial force and bending moment were calculated from strain gauge records. As the influence of friction on the axial force was small, the one at the GL-4.5 m point where the influence of the bending moment was small was used. The results were averaged for the left pile (P1, P3) and right pile (P2, P4) to eliminate the influence of the difference in the initial axial force due to the difference in pile position. The bending moment at each depth was extrapolated using cubic spline interpolation, and the bending moment at the GL-1.25 m point at the lower end of the pile cap was obtained. The solid black line and dashed line in Fig. 16 show the ultimate and short-term strength of the prototype cast-in-place concrete pile. Since the model pile during the experiment was within the elastic range, stress exceeded these load-bearing curves. As shown in Fig. 16, the significant input of 600 Gal generated stress that was large enough to break the pile. The correlation between the axial force and the bending moment was high in Cases 1-2 and 2-2 (Fig. 16(a), (b)), but the correlation was slightly disturbed in Case 3-1 (Fig. 16(c)). Furthermore, the range of each axial force was approximately -25 - +5 MN in Cases 1-2 and 3-1 (Fig. 16(a), (c)) and

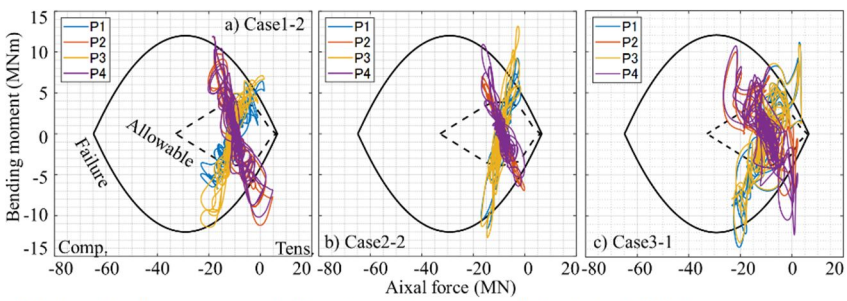

Fig. 16 Bending moment – axial force interaction curve at pile heads in 600Gal input

approximately -15 - ±0 MN in Case 2-2 (Fig. 16(b)). Meanwhile, the range of bending moment was about -12 to +12 MNm. From the above, although there were differences in the response between the building and the ground, the magnitude of the stress of the pile did not differ significantly except for the axial force of Case 2-2. The relationship between the incremental axial force that was estimated by Eq. (1) and the observed incremental axial force is shown in Fig. 17.

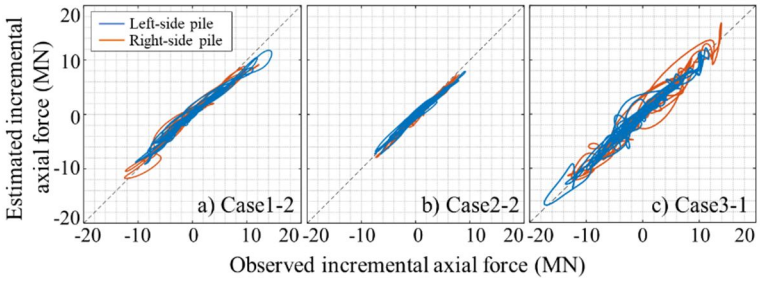

Fig. 17 Relationship of observed and estimated incremental axial force

$$P_i = (OTM + \sum M_i)/2L \qquad (1)$$

In Eq. (1), P_i is the incremental axial force (MN), OTM is the overturning moment (MNm), M_i is the pile head bending moment (MNm), and L is the inter-pile span (12 m). As shown in Fig. 17, the estimated incremental axial force is consistent with the observed total axial force, and the cumulative axial force could be calculated from the overturning moment and pile head bending moment. It is evident that Case 2-2 had a roughly similar pile head bending moment compared to that of Case 1-2 (Fig. 16(a), (b)). However, given that the overturning moment was smaller due to the liquefaction of the surface layer ground (Fig. 12(b)), the incremental axial force from Eq. (1) was smaller than that of Case 1-2. Furthermore, the pile head bending moment was approximately the same even though the inertial force was small at the 600 Gal inputs of Cases 1-2 and 2-2 (Fig. 12(a)). Fig. 18 shows the times at which the bending moments in the left and right directions were maximized for the ground displacement obtained from acceleration integration, and the pile displacement obtained by combining the acceleration integration of the foundation and upper end of the support layer, foundation rotation obtained from the displacement meter, and pile deformation obtained from the strain. Case 1-2 showed a large relative displacement between the pile and ground near the ground surface (Fig. 18(a1), (a2)), and it is inferred that the main ground reaction force of the pile was near the pile head. Meanwhile, Case 2-2 showed large ground deformation near GL-3.5 to 7.0 m due to liquefaction, and there was almost no relative displacement between piles shallower than GL-3.5 m and the ground, with relative displacement generated at GL-7.0 m and more profound (Fig. 18(b1), (b2)). It can be inferred from this that the main part of the ground reaction force in Case 2-2 was at a farther depth than the pile head. From the above results, it is thought that the increased ground deformation due to liquefaction in Case 2-2 resulted in a small ground reaction force near the surface layer and the generation of a ground reaction force at deeper positions, which is thought to have resulted in an almost equivalent pile head bending moment, even though the inertial force was smaller than that of Case 1-2. It is clear that the design that simultaneously applies the ground displacement increased due to liquefaction and the structural inertial force calculated in the non-liquefied state is on the safe side. However, a more rational pile design may be achieved by using the structural inertial force obtained from the damped structure acceleration by dynamic interaction analysis that considers liquefaction.

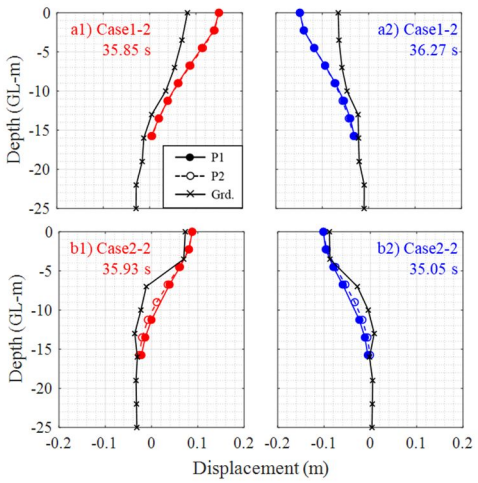

Fig. 18 Displacement distribution of pile and ground in Case1-2 and Case2-2

Because there was no significant difference in the axial force (Fig. 16(a), (c)) despite differences in the maximum overturning moment between Cases 1-2 and 3-1 (Fig. 12(b)), the relationship between the axial force and vertical displacement of the pile head is shown in Fig. 19. As shown in the figure, the vertical displacement increases sharply when the pile axial force reaches positive (tension side). Since the piles on the tension side of Cases 1-2 and 3-1 were pulled out due to a large overturning moment, the tension side axial force

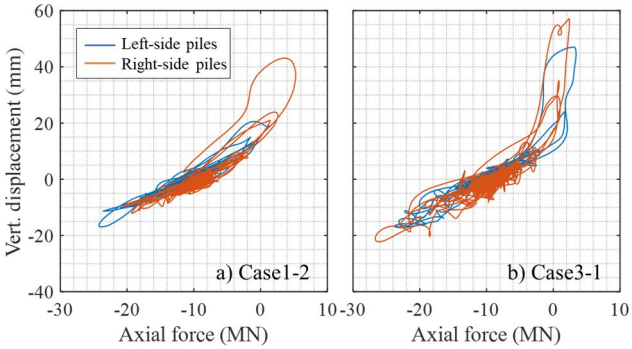

Fig. 19 Relationship of axial force and vertical displacement at pile head

peaked at the same level, and the couple compressive side axial force also peaked at the same level. Similarly, there was no significant difference in the maximum pile head bending moment (Fig. 16(a), (c)) despite differences in the maximum inertial force between Cases 1-2 and 3-1 (Fig. 12(b)). The enlarged part of the leading moving parts in the time history of the acceleration, inertial force, overturning moment, axial force, and pile head bending moment of the building top and foundation is shown in Fig. 20. The red line in the figure shows the time when the axial force peaks, and the blue line indicates the time when the pile head is bending moment peaks. Case 1-2 shows that the red and blue lines are relatively close, but Case 3-1 shows more space between the red and blue lines. In all cases, the acceleration at the top of the building peaked at the maximum time of the axial force indicated by the red line. The overturning moment also peaked; as such, no differences could be observed. However, Case 1-2 did not peak at the pile head bending moment shown by the blue line, and the inertial force of Case 3-1 peaks, which offers a difference. The phase difference between the swaying motion and rocking motion of the superstructure may have affected the pile head bending moment. That is, since the moment of inertia of the structure was small and the phases of the swaying and rocking motion were relatively close in Case 1-2, the pile head rotation affected the pile head bending moment in addition to the pile head inertial force. In contrast, as the moment of inertia of the structure was large and the phases of the swaying and rocking motion were separated in Case 3-1, the effect of the pile head rotation was small, and the pile head's bending moment peaked at the peak of the structural inertial force. As described above, since the maximum inertial force and maximum pile head bending moment did not occur at the same time in Case 1-2, it is thought that the pile head bending moment was approximately equal even though a more significant structural inertial force was generated than in Case 3-1.

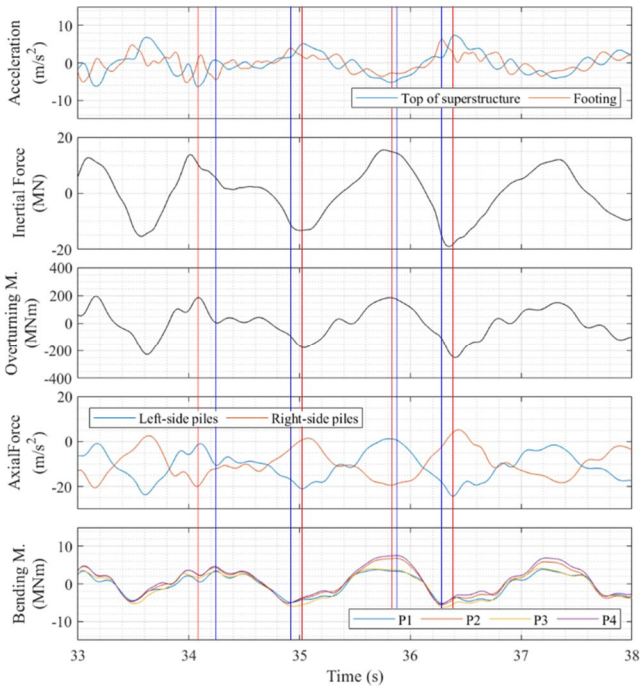

a) Case1-2

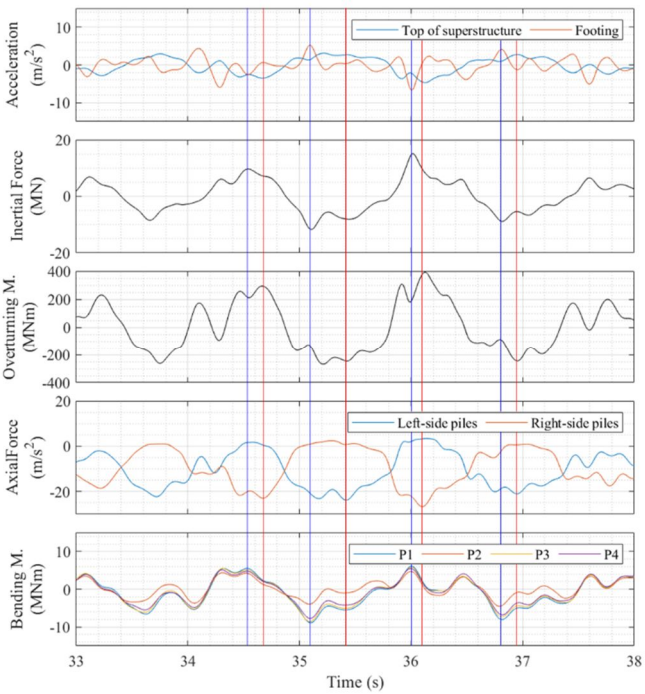

b) Case3-1

Fig. 20 Time records of acceleration, inertial force, overturning moment, axial force, and bending moment

To further discuss the effect of the phase shift between the swaying and rocking motion of the structure on the pile head stress as described above, the deformation of the model at the maximum bending moment and maximum axial force close to it, as well as the visualization of the inertial force at each point mass, is shown in Fig. 21. As shown in the figure, the inertial force of the foundation mass is significant at the peak of the pile head bending moment in all cases. This can be observed from the foundation acceleration peaks at the blue line time in Fig. 20. Meanwhile, the inertial force of the top point mass is large, and the inertial force of the foundation mass is almost zero when the axial force is at the maximum. Similarly, it can be observed from the fact that the top acceleration peaks at the red line time in Fig. 20, and the foundation acceleration decreases. This is also clear because, when considering the harmonic vibration in a multi-mass system with a fixed foundation, the foundation becomes a vibration node due to the superposition of the input wave and the reflected wave when the peak acceleration occurs at the top in the natural vibration mode. It is suggested from the above results that, although it is common to calculate the structural inertial force by adding the

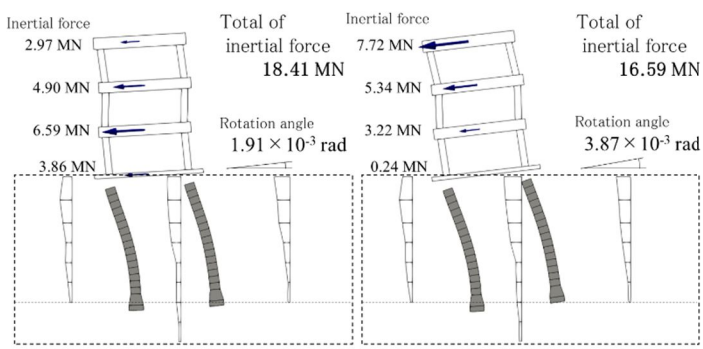

a1) At the time when the peak bending moment recorded in Case 1-2 (t = 36.29 s)

a2) At the time when the axial force recorded in Case 1-2 (t = 36.38 s)

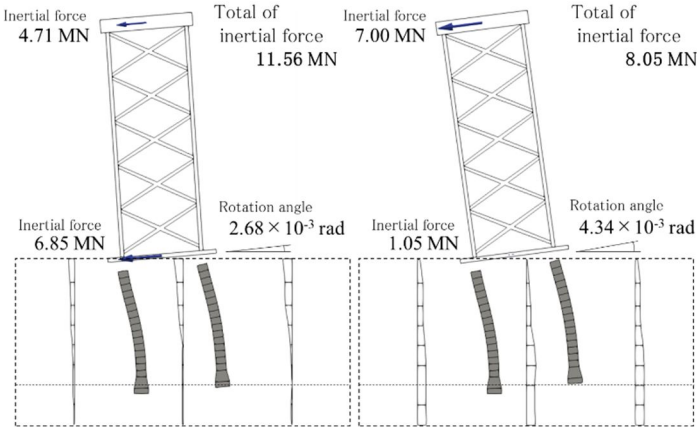

b1) At the time when the peak bending moment recorded in Case 3-1 (t = 35.09 s)

b2) At the time when the axial force recorded in Case 3-1 (t = 35.42 s)

Fig. 21 Schematic diagram visualized from centrifugal test data at the time when the peak axial force and bending moment were recorded. (The displacement is enlarged 30 times.)

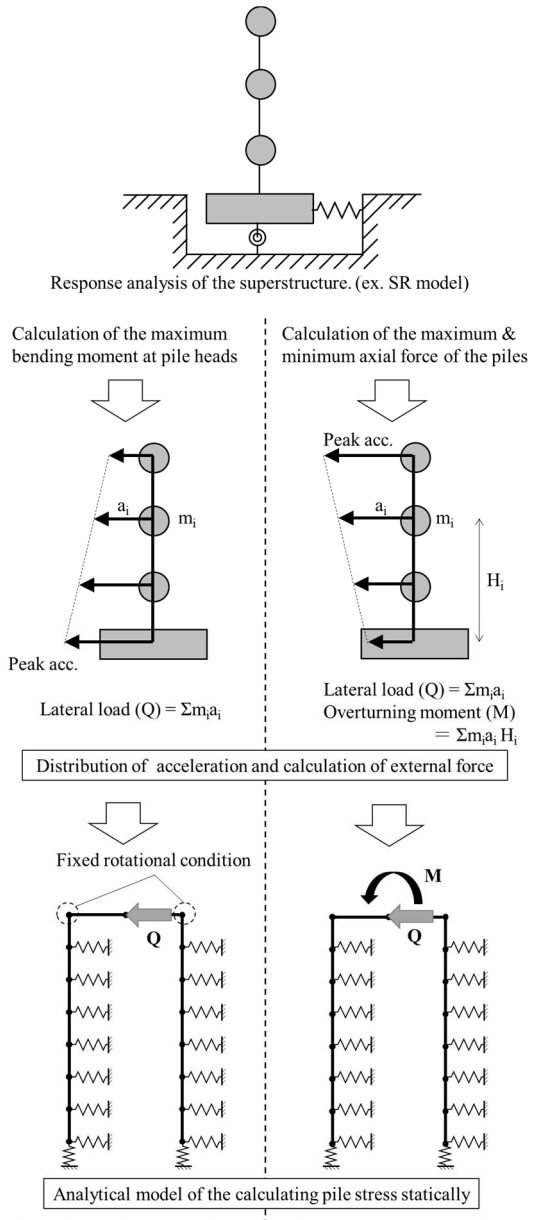

Fig. 22 Schematic diagram of the new analysis method considering structure-pile-ground interaction of plate-shaped building

maximum inertial force (layer shear force) from the foundation to the top of the building and the pile stress as the pile head rotation fixing condition as the A_i distribution when designing the pile foundation of a plate-shaped building, there is the possibility that a more rational design can be achieved by changing the load conditions and boundary conditions between the response calculation of the superstructure considering the dynamic interaction, bending moment calculation, and axial force calculation. Fig. 22 shows a conceptual diagram of this. The superstructure inertial force used when calculating the pile head bending moment is calculated when the acceleration of the foundation is maximized, and the pile head is fixed. Since there is some rotation of the pile head, in reality, it is possible that the safe side could be considered by fixing the rotation of the pile head. The superstructure inertial force and the overturning moment that is used when calculating the axial force were set at the time when the top acceleration is at the maximum, and the pile head was calculated as a multi-point constraint (rigid body connection).

5 Conclusion

This study investigated a method for establishing a soft clayey ground in a centrifugal model experiment to understand the dynamic behavior of a complex plate-shaped building–pile–clayey ground system during a large earthquake. Additionally, we conducted a dynamic centrifugal model experiment of a plate-shaped building–pile–clayey ground system using the obtained experimental method. The results obtained are as follows:

1) We used Kanto Loam as the cohesive soil material. We showed a method to efficiently manufacture a soft clayey ground stabilizing in a short period in a centrifugal field by controlling the maximum dry density and optimal water content ratio when manufacturing a model ground. Furthermore, we conducted vibration experiments using a ground-only test specimen that does

not contain a structure. We identified the ground rigidity and damping from the obtained acceleration to confirm that the centrifugal field's ground rigidity and non-linear characteristics were generally harmonious with the laboratory test results.

2) It was also concluded that there was damping of the building inertial force due to the more extended period of the ground due to liquefaction. Meanwhile, despite the small inertial force of the building due to the large ground deformation, the pile head bending moment was approximately the same as that of the non-liquefied ground. This shows that a more rational pile design could be achieved by obtaining the structural inertial force dampened by liquefaction using dynamic interaction analysis that considers liquefaction.
3) It was also concluded that an increased moment of inertia of the structure resulted in the phase difference widening between the swaying and rocking motions of the structure and the pile head bending moment reaching a maximum value when the inertial force of the foundation was maximized. The axial force reaching a maximum value when the inertial force at the top of the building was maximized. It was shown that, when calculating the pile head bending moment by obtaining the acceleration of the foundation and each floor by response analysis that considers rocking, a more rational pile design may be achieved by using the acceleration distribution when the foundation is maximized and the acceleration distribution when the acceleration at the top of the building is maximum for the axial force.

The above results are only for a single waveform and may differ for other vibrational waves such as long-period ground motion. Analytical study needs to be conducted since creating the same ground in an experiment is complex. It has been confirmed that highly reproducible results could be achieved by non-linear time-history response analysis using the three-dimensional finite element method[12]. Hence, we will proceed with verification by conducting analytical studies on other types of ground motion in the future.

Acknowledgements

This research was conducted as part of the Long-Lifespan Building System Promotion Project by the Long-Lifespan Building System Promotion Council. We received a grant from the Ministry of Land, Infrastructure, Transport, and Tourism to promote housing market development from FY2016 to FY2018. In promoting this research, we have received a great deal of support from the Long-Lifespan Building System Promotion Council and the Association of New Urban Housing Technology Long-Lifespan Building System Promotion Committee. We want to thank you for your support.

References

1) Architectural Institute of Japan: Response analysis and seismic design considering dynamic interaction between building and ground, Architectural Institute of Japan, pp. 1-18, 2009. (in Japanese)
2) Y. Sako and M. Yamazoe: Seismic performance of pile foundations revealed in E-defense experiments, and how to apply the lessons learned from earthquakes to research on ground motion, ground, and foundations, Architectural Institute of Japan Structural Committee/Vibration Steering Committee, pp. 68-78, 2018. (in Japanese)
3) M. Mori: Ground foundation vibration – elucidation of nonlinear dynamic interactions and incorporation into the design, Symposium "Five Years After the Great East Japan Earthquake: Achievements and Remaining Issues of Architectural Vibration Engineering", Architectural Institute of Japan Structural Committee / Vibration Steering Committee, pp. 25-32, 2016. (in Japanese)
4) R. Kishida, Y. Katsura, and S. Nishio: Shear wave velocity and Young's modulus of sandy ground by centrifugal model experiment, Shimizu Corporation Research Report, pp. 9-14, 1997. (in Japanese)
5) E. Kohama and T. Sugano: Centrifuge model test on the dynamic behavior of pile foundations in cohesive soil layers during earthquakes, 39th Japan National Conference on Geotechnical Engineering Proceedings, pp. 1791-1792, 2004. (in Japanese)
6) L. Zhang, S. H. Goh, and H. Liu: Seismic response of pile-raft-clay system subjected to a long-duration earthquake: centrifuge test and finite element analysis, Soil Dynamics and Earthquake Engineering, Vol. 92, pp.488-502, 2017.
7) T. K. Garala and G. S. P. Madabhushi: Seismic behavior of soft clay and its influence on the response of friction pile foundations, Bulletin of Earthquake Engineering, 17, pp.1919 - 1939, 2019.

8) T. Okumura, T. Honda, J. Hamada, and T. Tanikawa: Seismic response of soft clayey ground in a centrifugal model test, 52nd Japan National Conference on Geotechnical Engineering Proceedings, pp. 1223-1224, 2017. (in Japanese)
9) T. Kagawa: On the similitude in model vibration tests of earth-structures, Proceedings of the Japan Society of Civil Engineers, pp. 67-77, 1978. (in Japanese)
10) K. Nishi, T. Okumura, T. Honda, J. Hamada, and T. Tanikawa: Behavior of plate-shaped building foundations standing on the soft clayey ground during an earthquake, Part II: Centrifuge model experiment results, Summaries of Technical Papers of the Annual Meeting of the Architectural Institute of Japan, Vol. B-2, pp. 779-780, 2017. (in Japanese)
11) M. D. Trifunac: Low frequency digitization errors and a new method for zero baseline correction of strong-motion accelerograms, Technical report of Earthquake Engineering Research Laboratory, California Institute of Technology, 1970.
12) T. Okumura, T. Honda, and J. Hamada: Dynamic centrifuge model tests on pile foundation of plate-shape building in soft clayey ground and its numerical analyses, Journal of Japan Association for Earthquake Engineering, No. 19, Vol. 6, pp. 167-180, 2019. (in Japanese)